Supporting Information for

Advancing Isotope-Enabled Model for Comprehensive Understanding of Atmospheric Sulfur Isotope Effects: Revealing the Overlooked Isotopic Fractionation During Combustion and Gas Desulfurization

Lianfang Wei[1,2,3], Xueshun Chen[1], Wenyi Yang[4], Zhe Wang[1], Jie Li[1], Di Liu[1], Huiyun Du[1], Xiaole Pan[1], Yafang Cheng[3], Pingqing Fu[5], Zifa Wang[1,6*]*

[1] State Key Laboratory of Atmospheric Boundary Layer Physics and Atmospheric Chemistry, Institute of Atmospheric Physics, Chinese Academy of Sciences, Beijing 100029, China

[2] Chinese Research Academy of Environmental Sciences, Beijing 100012, China

[3] Aerosol Chemistry Department, Max Planck Institute for Chemistry, Mainz, Germany

[4] Center of Air Quality Simulation and System Analysis, Chinese Academy of Environmental Planning, Beijing 100012, China

[5] Institute of Surface-Earth System Science, School of Earth System Science, Tianjin University, Tianjin 300072, China

[6] University of Chinese Academy of Sciences, Beijing, 100049, China

Corresponding author: Pingqing Fu (fupingqing@tju.edu.cn), Zifa Wang (zifawang@mail.iap.ac.cn)

This supporting information document contains 19 pages with detailed descriptions of CTM and model configuration, the algorithm framework of the isotopic chemistry module, the derivation of the stable isotopic composition of a reservoir in open systems, additional data, 2 tables, 3 figures, and references.

Text S1 The description of CTMs and model configuration. The three-dimensional atmospheric chemical transport model (CTMs) solves the continuity equation for the chemical species for representing its entire cycle in the atmosphere, including emission, transport (e.g. diffusion, advection), chemical production/loss, dry and wet deposition processes. The general Eulerian form of the continuity equation can be expressed mathematically by

$$\frac{\partial \bar{c}}{\partial t} = -\nabla \cdot (\bar{c}\bar{U}) + \nabla \cdot (K\nabla \cdot \bar{c}) + [\frac{\partial \bar{c}}{\partial t}]_{Emis} + [\frac{\partial \bar{c}}{\partial t}]_{Chem} - [\frac{\partial \bar{c}}{\partial t}]_{Dry} - [\frac{\partial \bar{c}}{\partial t}]_{Wet}$$

where $\bar{c}$ is the time-averaged concentration of the chemical species of interest. The term on the left side is the temporal change of concentration. The first two terms on the right side are advection, and turbulent diffusion of the time-averaged flux, the last four terms represent the emission intensity, time-averaged rate of chemical interactions (including production and loss process), dry deposition, and wet scavenge. $\nabla = (\partial/\partial x, \partial/\partial y, \partial/\partial z)$ is the gradient vector, U = (u, v, w) is the local wind velocity vector, and K is a 3×3 matrix with zero values for the non-diagonal elements and with diagonal elements K_x, K_y, K_z representing the turbulent diffusion coefficients in each transport direction.

The model is initialized using gridded meteorological and emission input. The meteorological field is processed through the interpolation of NCEP FNL (Final) Operational Global Analysis and forecast dataset on 0.25° × 0.25° grids, employing the WRF (Weather Research and Forecast model, version 3.9). Anthropogenic emissions, including SO_2, NO_x, NH_3, CO, VOCs, black carbon, and organic carbon, are obtained from the fusion of Hemispheric Transport of Air Pollution version-2 (HTAPv2) at a 1° horizontal resolution for the year 2010 (Janssens-Maenhout et al., 2015), and the Multi-resolution Emission Inventory for China (MEIC) at a 0.1°× 0.1° horizontal

resolution for the year 2015 (Li et al., 2017). The emission inventory for the Chinese region is overwritten with the MEIC. The online mineral dust is based on the wind erosion model developed by Wang et al. (2000) and the sea salt emissions parameterizations are referenced from Athanasopoulou et al. (2008), respectively.

The Rapid Radiative Transfer Model for General Circulation Model (RRTMG) scheme is employed for the computation of longwave and shortwave atmospheric radiative fluxes and heating rates (Pincus et al., 2003). The Madronich F-TUV (Fast Tropospheric Ultraviolet-Visible) scheme is utilized to estimate the photolysis rate. The WSM3 scheme (Hong et al., 2004) is selected for microphysics schemes. For the surface layer and boundary layer evaluations, the Monin-Obukhov scheme (Monin and Obukhov, 1954) and the Yonsei University (YSU) scheme (Hong et al., 2006) are chosen, respectively.

The Carbon Bond Mechanism version Z (CBM-Z) is employed for the gas-phase chemistry scheme (Zaveri and Peters, 1999). The aqueous chemistry module is taken from Regional Acid Deposition Model (RADM2) (Stockwell et al., 1997), including sulfur chemistry and a simple mechanism for wet scavenging. The dry deposition process is parameterized through the calculation of deposition velocity, employing the resistance model approach developed by Zhang et al. (2003). Recently, the Global Nested Grid Air Quality Prediction Model System (GNAQPMS) has been coupled with the CAS earth system model (CAS-ESM) (Wei et al., 2019). It shows good performance on the global budgets and spatial distribution of major atmospheric species, as validated against field observations and other model results. The oxidation processes of S(IV) to S(VI) involve gas-phase oxidation by SO_2 and OH radical, as well as aqueous phase oxidation through dissoluble S(IV) with O_3, H_2O_2, NO_2, and proxy acetic acid (CH_3OOH), along

with transition metal-catalyzed O_2 in cloud water. The oxidation of S(IV) species by dissolved NO_2 is also incorporated into the sulfur aqueous chemistry, referring to the kinetic parameters proposed by Cheng et al. (2016). The bulk cloud water pH is iteratively calculated online using the electroneutrality equation, considering concentrations of anions (sulfate, sulfite, nitrate, carbonate, formic acid) and cations (NH_4^+, Ca^{2+}, Mg^{2+}, Mn^{2+}, Fe^{3+}). Ion concentrations are determined based on Henry's law, dissociation equilibrium and ionization processes. Neutralized cations are mainly contributed by dust aerosol, with natural dust materials assumed to contain 10 wt% of Ca^{2+}, 3 wt% of Mg^{2+}, 0.5 wt% of Mn^{2+} and 0.5 wt% of Fe^{3+} (Wang et al., 2002). The gas–particle partitioning of inorganic aerosols and aerosol water content is simulated using the improved thermodynamic equilibrium module ISORROPIA II (Fountoukis and Nenes, 2007; Song et al., 2018). Refer to Table S2 for a comprehensive description of the model configuration.

The current implementation of the isotopic chemistry module relies on several assumptions. (1) The pollutants and cloud water are uniformly distributed within the grid cell. (2) During wet scavenging and dry deposition, no isotopic fractionation occurs, the small mass change due to isotopic substation is insignificant relative to the mass of particle, therefore, we apply the same K_j to ^{32}S and ^{34}S due to their similar molecular mass. (3) The model does not account for variations in isotopic composition from different emission sources. Instead, we focus on model's ability to reproduce the isotope effect, thus the isotopic composition of SO_2 and sulfate from emission sources are simply set to 0‰. The treatment does not influence the comparison between simulated and observed sulfur isotope effect during oxidation processes.

Text S2 The algorithm framework of isotopic chemistry module

We initially track the net change of SO_2 and sulfate after gas-phase, heterogeneous, and cloud&aqueous chemistry module separately, and then determine the reaction fraction *f* of SO_2 with each specific oxidation pathway during every time step (Δt) to be used as input for the isotope chemistry module. At each time step, the temperature and the temperature-dependent isotopic fractionation factor at the grid cell are updated.

To reduce the effect of time-dependent Rayleigh equation with a large reaction fraction. The iterative time-splitting technique is employed. Within each sub-timestep, the reaction fraction is set at 1%, and a repetition involves adding equal portions of a fresh mixture. Utilizing the input mass of sulfur-containing isotopologues $^{32}SO_2$ and $^{34}SO_2$ at the last time step as initial value, we calculate the isotope ratio of $^{32}SO_4^{2-}$ and $^{34}SO_4^{2-}$ in the product, as well as the isotope ratio of $^{32}SO_2$ and $^{34}SO_2$ in the remaining reactant based on Rayleigh equations. We then derive the net mass change of $^{32}SO_2$, $^{34}SO_2$, $^{32}SO_4^{2-}$ and $^{34}SO_4^{2-}$ using the isotopic mass balance at each sub-timestep, as expressed in the following equation.

$$\Delta MC\left(\,^{l}X\right)_t = \left(MC\left(\,^{h}X\right)_{S_{t-1}} - R\left(\,^{h}X/\,^{l}X\right)_{S_t} \times MC\left(\,^{l}X\right)_{S_{t-1}}\right) \Big/ \left(R\left(\,^{h}X/\,^{l}X\right)_{P_t} - R\left(\,^{h}X/\,^{l}X\right)_{S_t}\right)$$

$$\Delta MC\left(\,^{h}X\right)_t = R\left(\,^{h}X/\,^{l}X\right)_{P_t} \times \Delta MC\left(\,^{l}X\right)_t$$

Where $\Delta MC\left(\,^{h}X\right)_t$ and $\Delta MC\left(\,^{l}X\right)_t$ represent the change in molar mass of isotopologues containing heavy ^{h}X and light isotope ^{l}X of element X at time t during the chemical process, respectively. $MC\left(\,^{h}X\right)_{S_{t-1}}$ and $MC\left(\,^{l}X\right)_{S_{t-1}}$ represent the molar mass of reactant *S* containing heavy $^{h}X$and light isotope ^{l}X of element X at time t-1, respectively.

During each sub-timestep, the isotope ratio of the substrate is updated with the new mixing, and the isotope ratio of the accumulated product is weighted with the molar mass and isotope ratio of the product at each sub-timestep. An iterative loop is executed for the above steps.

Text S3 The derivation of stable isotopic composition of a reservoir in open systems.

We consider a reservoir that loses material due to any physicochemical process with isotopic fractionation at a constant temperature. At any instant, the stable isotope ratio is given by

$$\mathrm{R} = \frac{N^*}{N} \quad \text{...(S1)}$$

Taking the logarithm of both sides of eq. (S1)

$$\ln R = \ln N^* - \ln N \quad \text{...(S2)}$$

After differentiating, eq. (S2) becomes

$$\frac{dR}{R} = \frac{dN^*}{N^*} - \frac{dN}{N} = \frac{dN^*}{NR} - \frac{dN}{N} \quad \text{...(S3)}$$

At any instant, let dN_e^* and dN_e are being lost and dN_r^* and dN_r are being added to the reservoir. So, the net change in N* and N is

$$dN^* = dN_r^* - dN_e^*$$
$$dN = dN_r - dN_e \quad \text{...(S4), (S5)}$$

Dividing eq. (S4) by eq. (S5)

$$\frac{dN^*}{dN} = \frac{dN_r^* - dN_e^*}{dN_r - dN_e} = \frac{\frac{dN_r^*}{dN_r} \times \frac{dN_r}{dN_e} - \frac{dN_e^*}{dN_e}}{\frac{dN_r}{dN_e} - 1} = \frac{\beta R_r - \alpha R}{\beta - 1} \quad \text{...(S6)}$$

Where α is defined as $(dN_e^*/dN_e)/(N^*/N)$, and β is dN_r/dN_e, the ratio of the amount of material added to that lost.

Substituting the value of dN^* from eq. (S6) to eq. (S3)

$$\frac{dR}{R} = \left(\frac{\beta R_r - \alpha R}{\beta - 1}\right) \times \frac{dN}{NR} - \frac{dN}{N} = \frac{dN}{N} \times \left(\frac{\beta \frac{R_r}{R}}{\beta - 1} - \frac{\alpha}{\beta - 1} - 1\right) \quad \text{...(S7)}$$

or

$$\frac{dR}{\left(\frac{\beta R_r}{\beta - 1} - \left(\frac{\alpha}{\beta - 1} + 1\right) \times R\right)} = \frac{dN}{N} \quad \text{...(S8)}$$

Taking integration on both sides

$$\frac{1}{-\left(\frac{\alpha}{\beta - 1} + 1\right)} \int \frac{d\left\{\frac{\beta R_r}{\beta - 1} - \left(\frac{\alpha}{\beta - 1} + 1\right) \times R\right\}}{\left\{\frac{\beta R_r}{\beta - 1} - \left(\frac{\alpha}{\beta - 1} + 1\right) \times R\right\}} = \int \frac{dN}{N} \quad \text{...(S9)}$$

The condition for integrating this equation is

$\frac{\beta R_r}{\beta - 1} \neq \left(\frac{\alpha}{\beta - 1} + 1\right) \times R$, it gives that $\frac{dN_r}{dN_e} \neq \left(\frac{\alpha - 1}{\frac{R_r}{R} - 1}\right)$

At β=1, this equation is not solvable, hence first we take the case where β≠1.

Case 1: on integrating eq. (S8), we get

$$\frac{1}{-\left(\frac{\alpha}{\beta - 1} + 1\right)} \times \ln\left\{\frac{\beta R_r}{\beta - 1} - \left(\frac{\alpha}{\beta - 1} + 1\right) \times R\right\} = \ln N + k \quad \text{...(S10)}$$

After applying boundary conditions, at t=1, $N=N_0$, $R=R_0$, we evaluate *k* and substitute in eq. (S10); we get

$$\frac{1}{-\left(\frac{\alpha}{\beta - 1} + 1\right)} \times \ln\left\{\frac{\left\{\frac{\beta R_r}{\beta - 1} - \left(\frac{\alpha}{\beta - 1} + 1\right) \times R\right\}}{\left\{\frac{\beta R_r}{\beta - 1} - \left(\frac{\alpha}{\beta - 1} + 1\right) \times R_0\right\}}\right\} = \ln \frac{N}{N_0} = \ln f \quad \text{...(S11)}$$

Here f is the fraction of the material left in the reservoir relative to the initial amount, which is difined as $(N^* + N)/ (N_0^* + N_0)$

Further simplifying eq. (S11) becomes

$$\mathrm{R} = R_0 f^{-\left(\frac{\alpha}{\beta - 1} + 1\right)} + \frac{\beta}{\alpha + \beta - 1} \times R_r \times \left[1 - f^{-\left(\frac{\alpha}{\beta - 1} + 1\right)}\right] \quad \text{...(S12)}$$

or

$$\mathrm{R} = R_0 f^{\rho} + \frac{\beta}{\alpha+\beta-1} \times R_r \times [1 - f^{\rho}] \quad \ldots(S13)$$

Here $\rho = -(\frac{\alpha}{\beta-1} + 1)$

Substituting β=0, eq. (S13) converts to the simple Rayleigh equation, which cross-checks the derivation.

$$\mathrm{R} = R_0 f^{(\alpha-1)} \quad \ldots(S14)$$

Case 2: When β=1, dN = 0 hence from eq. (S5), $dN_r = dN_e$. Equation (S3) becomes

$$\mathrm{dR} = \frac{dN_r^* - dN_e^*}{N} = R_r \frac{dN_r}{N} - \alpha R \frac{dN_e}{N} = \left(\frac{R_r - \alpha R}{N}\right) dN_r = \left(\frac{R_r - \alpha R}{N_0}\right) dN_r \quad \ldots(S15)$$

After rearranging and integrating, this becomes

$$-\frac{1}{\alpha} \int \frac{d(R_r - \alpha R)}{R_r - \alpha R} = \frac{1}{N_0} \int dN_r \quad \ldots(S16)$$

After solving fully and applying boundary conditions as in the previous case, we get

$$\mathrm{R} = R_0 exp[-(\alpha N_r / N_0)] + (R_r/\alpha) \times \{1 - exp[-(\alpha N_r / N_0)]\} \quad \ldots(S17)$$

Here N_r indicates the total number of lighter isotopeic molecules added thus far.

Table S1 Compiled observation data of $\delta^{34}S$ values of coal, sulfate aerosol, and wet precipitation across different Chinese provinces

Province	$\delta^{34}S$ of coal	$\delta^{34}S$ of wet precipitation	$\delta^{34}S$ of aerosol
Beijing	7.4±16.1	4.7±1.8	6.1±1.3
Tianjin			4.1±1.6
Inner Mongolia	0.8		
Heilongjiang	3.2±1.8		6.4
Liaoning	9.4±3.2		5.9
Jilin	1.7		8.1
Hebei	3.5±6.6		
Henan	6.4±1.0	2.1±2.3	
Shandong	7.6±2.9		
Gansu	7.3±3.5		
Zhejiang	4.0±1.5		6.2±2.7
Jiangsu	3.8±1.3		5.5±1.0
Anwei	3.8		
Fujian			3.5±1.1
Chongqing		4.3±1.1	
Jiangxi	-4.4±1.3		
Sichuan	8.8±1.3	3.9	
Shaanxi	7.9±4.6	12.3±1.1	
Shanxi	12.1±10.8		
Hubei	12.1		
Hunan	-6.6±5.7		
Guangdong	9.6±1.0		5.2±1.6
Guizhou	-7.5±0.1	-2.8±9.8	1.2
Yunnan	-0.7		

The dataset (Mean±std.) are compiled from references.

The compiled data from various Chinese provinces are cited from sources such as Beijing (Fan et al., 2020; Wei et al., 2018; Han et al., 2016b; Hong et al., 1993; Maruyama et al., 2000; Ohizumi et al., 1997; Mukai et al., 2001; Han et al., 2016a; Zhu et al., 2016), Tianjin (Han et al., 2022; Ding et al., 2022), Inner Mongolia (Hong et al., 1993), Heilongjiang (Hong et al., 1993; Ohizumi et al., 1997; Mukai et al., 2001), Liaoning (Hong et al., 1993; Maruyama et al., 2000; Ohizumi et al., 1997), Jilin

(Hong et al., 1993; Mukai et al., 2001), Hebei (Hong et al., 1993), Henan (Hong et al., 1993; Zheng et al., 2024), Shandong (Hong et al., 1993), Gansu (Xiao and Liu, 2011), Zhejiang (Hong et al., 1993; Lin et al., 2022), Jiangsu (Hong et al., 1993; Chen et al., 2017; Li et al., 2020; Maruyama et al., 2000; Mukai et al., 2001), Anwei (Hong et al., 1993), Fujian (Lin et al., 2019), Chongqing (Xiao et al., 2009; Wu and Han, 2015), Jiangxi (Hong et al., 1993; Xiao and Liu, 2011; Xiao et al., 2009), Sichuan (Hong et al., 1993; Xiao et al., 2009), Shaanxi (Xiao and Liu, 2011; Bai and Wang, 2014), Shanxi (Xiao and Liu, 2011; Maruyama et al., 2000; Ohizumi et al., 1997), Hubei (Xiao and Liu, 2011), Hunan (Hong et al., 1993; Xiao and Liu, 2011), Guangdong (Lin et al., 2019), Guizhou (Hong et al., 1993; Mukai et al., 2001; Xiao et al., 2009; Xiao et al., 2014), Yunnan (Hong et al., 1993)

186 **Table S2 The detailed information of model configurations**

Module	Parameterizations/schemes
Input global analysis data	NCEP GDAS/FNL data
Gas-phase chemical mechanism	CBM-Z mechanism (Zaveri and Peters, 1999)
Aqueous-phase chemical mechanism and wet scavenge	RADM mechanism (Chang et al., 1987)
Anthropogenic emissions	HTAPv2 and MEIC
Dust, sea salt	wind erosion model (Wang et al., 2000) sea salt online parameterization (Athanasopoulou et al., 2008)
Photolysis scheme	Madronich F-TUV
Microphysics scheme	WSM3 (Hong et al., 2004)
Longwave radiation scheme	RRTM (Mlawer et al., 1997)
Shortwave radiation scheme	Dudhia scheme (Dudhia, 1989)
Surface layer	Monin-Obukhov (Janjic) scheme (Monin and Obukhov, 1954)
Land surface schemes	NOAH (Ek et al., 2003)
Planetary boundary layer physics	YSU scheme (Hong et al., 2006)
Cumulus	Kain-Fritsch scheme (Kain and Kain, 2004)
Vertical layers	20

187

188

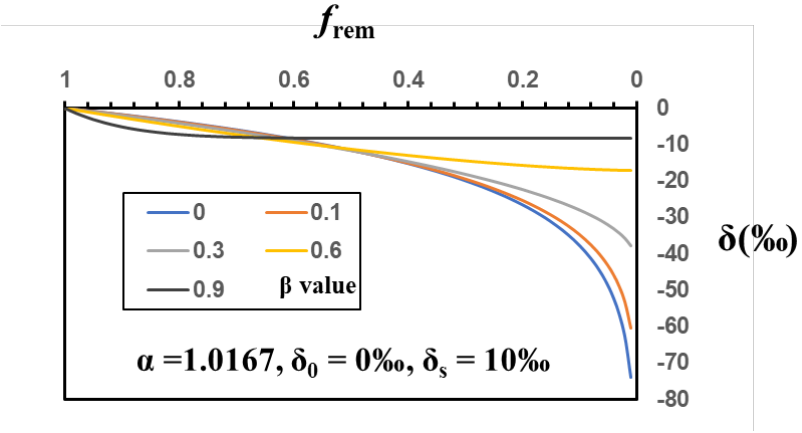

Figure S1. An example illustrating the change in isotopic composition (δ) of a reservoir related to the remaining fraction (f_{rem}) of the original material, considering various values of β, which represents the ratio of the instantaneous amount added to the removal during an infinitesimal time interval Δt (β≠1). The isotopic composition of the external source (δ_s) is assumed to be 10‰, and the fractionation factor is set to 1.0167.

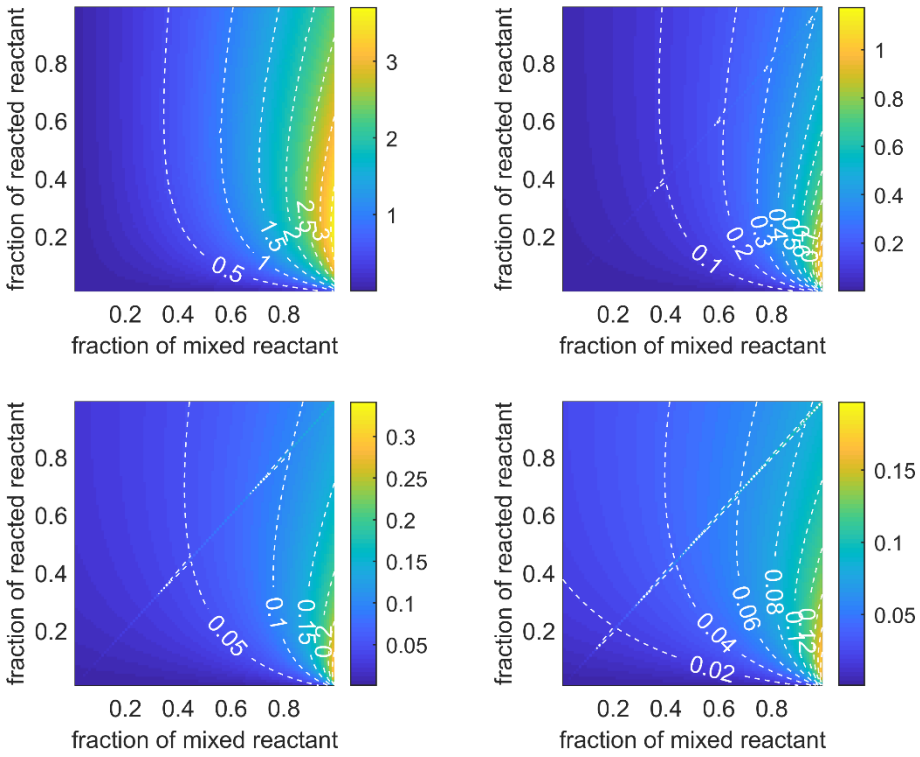

197

198 **Figure S2**. Simulation deviation of the isotopic composition of reservoir for varying
199 sub-steps (a) 1, (b) 10, (c) 50, and (d) 100, relative to reference simulation with
200 integration method in the open system associated with simultaneous reaction and
201 mixing processes. Each simulation involves the addition of a compound with an initial
202 δ-value of 10.0‰ to the substrate (initially δ= 0‰), while the chemical reaction
203 exhibits an isotopic effect with a fractionation factor of α= 1.0167. The fractions of
204 added and removed products range from 1% to 99% of the initial amount of substrate
205 and are uniformly divided at every time sub-step. The color scheme and contour lines
206 illustrate the δ-value differences between the respective simulations and the
207 referenced simulation.

208

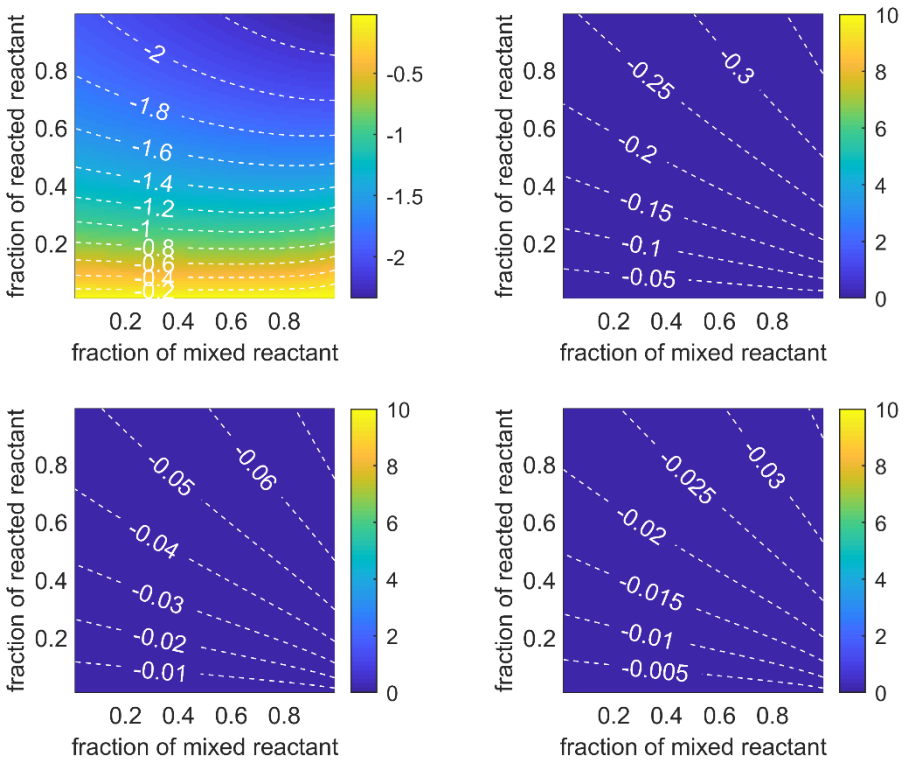

209

210 **Figure S3.** Simulation deviation of the isotopic composition of the product for varying
211 sub-steps (a) 1, (b) 10, (c) 50, and (d) 100, relative to reference simulation with 1000
212 sub-steps. Each simulation involves the addition of a compound with an initial δ-value
213 of 10.0‰ to the substrate (initially δ = 0‰), while the chemical reaction exhibits an
214 isotopic effect with a fractionation factor of α= 1.0167. The fractions of added and
215 removed products range from 1% to 99% of the initial amount of substrate and are
216 uniformly divided at every time sub-step. The color scheme and contour lines illustrate
217 the δ-value differences between the respective simulations and the referenced
218 simulation.

219

References

National Centers for Environmental Prediction/National Weather Service/NOAA/U.S. Department of Commerce, NCEP GDAS/FNL 0.25 Degree Global Tropospheric Analyses and Forecast Grids, Research Data Archive at the National Center for Atmospheric Research, Computational and Information Systems Laboratory, 2015, updated daily. DOI: 2010.5065/D2065Q2014T2014Z (accessed 2022/2012/2015). DOI: 10.5065/D65Q4T4Z (accessed 2022/12/5),

Athanasopoulou, E., Tombrou, M., Pandis, S., and Russell, A.: The role of sea-salt emissions and heterogeneous chemistry in the air quality of polluted coastal areas, Atmos. Chem. Phys., 8, 5755-5769, 2008.

Bai, L. and Wang, Z.-L.: Anthropogenic influence on rainwater in the Xi'an City, Northwest China: Constraints from sulfur isotope and trace elements analyses, Journal of Geochemical Exploration, 137, 65-72, 10.1016/j.gexplo.2013.11.011, 2014.

Chen, S. L., Guo, Z. Y., Guo, Z. B., Guo, Q. J., Zhang, Y. L., Zhu, B., and Zhang, H. X.: Sulfur isotopic fractionation and its implication: Sulfate formation in PM2.5 and coal combustion under different conditions, Atmospheric Research, 194, 142-149, 10.1016/j.atmosres.2017.04.034, 2017.

Cheng, Y., Zheng, G., Wei, C., Mu, Q., Zheng, B., Wang, Z., Gao, M., Zhang, Q., He, K., and Carmichael, G.: Reactive nitrogen chemistry in aerosol water as a source of sulfate during haze events in China, Sci. Adv., 2, e1601530, 2016.

Ding, S., Chen, Y., Li, Q., and Li, X.-D.: Using Stable Sulfur Isotope to Trace Sulfur Oxidation Pathways during the Winter of 2017–2019 in Tianjin, North China, International Journal of Environmental Research and Public Health, 19, 10966, 2022.

Fan, M.-Y., Zhang, Y.-L., Lin, Y.-C., Li, J., Cheng, H., An, N., Sun, Y., Qiu, Y., Cao, F., and Fu, P.: Roles of sulfur oxidation pathways in the variability in stable sulfur isotopic composition of sulfate aerosols at an urban site in Beijing, China, Environ. Sci. Technol. Lett., 7, 883-888, 2020.

Fountoukis, C. and Nenes, A.: ISORROPIA II: a computationally efficient thermodynamic equilibrium model for K^+–Ca^{2+}–Mg^{2+}–NH_4^+–Na^+–SO_4^{2-}–NO_3^-–Cl^-–H_2O aerosols, Atmos. Chem. Phys., 7, 4639-4659, 2007.

Han, X., Lang, Y., Guo, Q., Li, X., Ding, H., and Li, S.: Enhanced Oxidation of SO2 by H2O2 During Haze Events: Constraints From Sulfur Isotopes, Journal of Geophysical Research: Atmospheres, 127, e2022JD036960, 2022.

Han, X., Guo, Q., Liu, C., Fu, P., Strauss, H., Yang, J., Hu, J., Wei, L., Ren, H., and Peters, M.: Using stable isotopes to trace sources and formation processes of sulfate aerosols from Beijing, China, Sci. Rep., 6, 2016a.

Han, X., Guo, Q., Liu, C., Strauss, H., Yang, J., Hu, J., Wei, R., Tian, L., Kong, J., and Peters, M.: Effect of the pollution control measures on $PM_{2.5}$ during the 2015 China Victory Day Parade: Implication from water-soluble ions and sulfur isotope, Environ. Pollut., 218, 230-241, 2016b.

Hong, S.-Y., Dudhia, J., and Chen, S.-H.: A revised approach to ice microphysical processes for the bulk parameterization of clouds and precipitation, Monthly weather review, 132, 103-120, 2004.

Hong, S.-Y., Noh, Y., and Dudhia, J.: A new vertical diffusion package with an explicit treatment of entrainment processes, Monthly weather review, 134, 2318-2341, 2006.

Hong, Y., Zhang, H., and Zhu, Y.: Sulfur isotopic characteristics of coal in China and sulfur isotopic fractionation during coal-burning process, Chinese Journal of Geochemistry, 12, 51-59, 1993.

Janssens-Maenhout, G., Crippa, M., Guizzardi, D., Dentener, F., Muntean, M., Pouliot, G., Keating, T., Zhang, Q., Kurokawa, J., and Wankmüller, R.: HTAP_v2. 2: a mosaic of regional and global emission grid maps for 2008 and 2010 to study hemispheric transport of air pollution, Atmos. Chem. Phys., 15, 11411-11432, 2015.

Li, J., Zhang, Y.-L., Cao, F., Zhang, W., Fan, M., Lee, X., and Michalski, G.: Stable sulfur isotopes revealed a major role of transition-metal ion-catalyzed SO_2 oxidation in haze episodes, Environ. Sci. Technol., 54, 2626-2634, 2020.

Li, M., Zhang, Q., Kurokawa, J.-i., Woo, J.-H., He, K., Lu, Z., Ohara, T., Song, Y., Streets, D. G., and Carmichael, G. R.: MIX: a mosaic Asian anthropogenic emission inventory under the international collaboration framework of the MICS-Asia and HTAP, Atmos. Chem. Phys., 17, 935-963, 2017.

Lin, M., T, M. H., Lin, M., Li, M., and Pnas, B. S.: Five-S-isotope evidence of two distinct mass-independent sulfur isotope effects and implications for the modern and Archean atmospheres, 2019.

Lin, Y.-C., Yu, M., Xie, F., and Zhang, Y.: Anthropogenic emission sources of sulfate aerosols in Hangzhou, East China: insights from isotope techniques with consideration of fractionation effects between gas-to-particle transformations, Environ. Sci. Technol., 56, 3905-3914, 2022.

Maruyama, T., Ohizumi, T., Taneoka, Y., Minami, N., Fukuzaki, N., Mukai, H., Murano, K., and Kusakabe, M.: Sulfur isotope ratios of coals and oils used in China and Japan, Nippon Kagaku Kaishi, 45-51, 10.1246/nikkashi.2000.45, 2000.

Monin, A. and Obukhov, A.: Osnovnye zakonomernosti turbulentnogo peremeshivanija v prizemnom sloe atmosfery (Basic laws of turbulent mixing in the atmosphere near the ground), Trudy geofiz. inst. AN SSSR, 24, 163-187, 1954.

Mukai, H., Tanaka, A., Fujii, T., Zeng, Y. Q., Hong, Y. T., Tang, J., Guo, S., Xue, H. S., Sun, Z. L., Zhou, J. T., Xue, D. M., Zhao, J., Zhai, G. H., Gu, J. L., and Zhai, P. Y.: Regional characteristics of sulfur and lead isotope ratios in the atmosphere at several Chinese urban sites, Environ. Sci. Technol., 35, 1064-1071, 10.1021/es001399u, 2001.

Ohizumi, T., Fukuzaki, N., and Kusakabe, M.: Sulfur isotopic view on the sources of sulfur in atmospheric fallout along the coast of the Sea of Japan, Atmos. Environ., 31, 1339-1348, 10.1016/s1352-2310(96)00278-6, 1997.

Pincus, R., Barker, H. W., and Morcrette, J. J.: A fast, flexible, approximate technique for computing radiative transfer in inhomogeneous cloud fields, Journal of Geophysical Research: Atmospheres, 108, 2003.

Song, S., Gao, M., Xu, W., Shao, J., Shi, G., Wang, S., Wang, Y., Sun, Y., and McElroy, M.

B.: Fine-particle pH for Beijing winter haze as inferred from different thermodynamic equilibrium models, Atmos. Chem. Phys., 18, 7423-7438, 10.5194/acp-18-7423-2018, 2018.

Stockwell, W. R., Kirchner, F., Kuhn, M., and Seefeld, S.: A new mechanism for regional atmospheric chemistry modeling, Journal of Geophysical Research: Atmospheres, 102, 25847-25879, 1997.

Wang, Z., Akimoto, H., and Uno, I.: Neutralization of soil aerosol and its impact on the distribution of acid rain over east Asia: Observations and model results, Journal of Geophysical Research: Atmospheres, 107, ACH 6-1-ACH 6-12, 2002.

Wang, Z., Ueda, H., and Huang, M.: A deflation module for use in modeling long-range transport of yellow sand over East Asia, Journal of Geophysical Research: Atmospheres, 105, 26947-26959, 2000.

Wei, L., Yue, S., Zhao, W., Yang, W., Zhang, Y., Ren, L., Han, X., Guo, Q., Sun, Y., Wang, Z., and Fu, P.: Stable sulfur isotope ratios and chemical compositions of fine aerosols ($PM_{2.5}$) in Beijing, China, Sci. Total Environ., 633, 1156-1164, https://doi.org/10.1016/j.scitotenv.2018.03.153, 2018.

Wei, Y., Chen, X., Chen, H., Li, J., Wang, Z., Yang, W., Ge, B., Du, H., Hao, J., and Wang, W.: IAP-AACM v1. 0: a global to regional evaluation of the atmospheric chemistry model in CAS-ESM, Atmos. Chem. Phys., 19, 8269-8296, 2019.

Wu, Q. X. and Han, G. L.: Sulfur isotope and chemical composition of the rainwater at the Three Gorges Reservoir, Atmospheric Research, 155, 130-140, 10.1016/j.atmosres.2014.11.020, 2015.

Xiao, H.-Y. and Liu, C.-Q.: The elemental and isotopic composition of sulfur and nitrogen in Chinese coals, Organic Geochemistry, 42, 84-93, 10.1016/j.orggeochem.2010.10.011, 2011.

Xiao, H.-Y., Tang, C.-G., Xiao, H.-W., Liu, X.-Y., and Liu, C.-Q.: Identifying the change in atmospheric sulfur sources in China using isotopic ratios in mosses, J. Geophys. Res-Atmos., 114, 10.1029/2009jd012034, 2009.

Xiao, H. W., Xiao, H. Y., Long, A. M., Wang, Y. L., and Liu, C. Q.: Sources and

meteorological factors that control seasonal variation of delta S-34 values in rainwater, Atmospheric Research, 149, 154-165, 10.1016/j.atmosres.2014.06.003, 2014.

Zaveri, R. A. and Peters, L. K.: A new lumped structure photochemical mechanism for large-scale applications, Journal of Geophysical Research: Atmospheres, 104, 30387-30415, 1999.

Zhang, L., Brook, J. R., and Vet, R.: A revised parameterization for gaseous dry deposition in air-quality models, Atmos. Chem. Phys., 3, 2067-2082, 2003.

Zheng, M., Song, D., Zhang, D., and Zhao, Z.: Variability of sulfur and oxygen isotope values within wet precipitation and its correlation with diminished anthropogenic sulfur dioxide (SO_2) emission, Atmos. Environ., 317, 120185, 2024.

Zhu, G., Guo, Q., Chen, T., Lang, Y., Peters, M., Tian, L., Zhang, H., and Wang, C.: Chemical and sulfur isotopic composition of precipitation in Beijing, China, Environmental Science and Pollution Research, 23, 5507-5515, 10.1007/s11356-015-5746-2, 2016.